

University of Applied Sciences

**HOCHSCHULE
EMDEN·LEER**



Carl von Ossietzky Universität Oldenburg

Institute of Physics

Practical training: 5.04.4671 Tools in Advanced Photonics
Markus Schellenberg

TAP-3 Electronic Speckle Pattern Interferometry

Felipe Bizarro Nini - 6492157
Mohammed Jasir Thai Valappil - 6444697

Summer semester 2023

Abstract

The aim of this laboratory practice is to get familiarized with Electronic Speckle Pattern Interferometry (ESPI) and its capabilities of detecting small deformations at the surface of a work-piece. Moreover, the experiment allows an insightful grasp onto the challenges of designing a optical setup given the desired measurement. With ESPI it was possible to determine the 3D deformation profile of a surface with precision of the order of less than 70 nm over an area of $8.9 \times 6.7 \text{ mm}^2$.

1 Introduction

When coherent light impinges onto a rough surface, light is scattered to many directions. Different rays arriving onto a detector will travel different distances and thus, a granular texture is formed on top of the captured image of the observed object. This noise depicted in Figure 1 is known as Speckle Pattern [4].



Figure 1: Granular texture of a speckle pattern produced by a HeNe laser shining onto a sheet of paper captured by a CCD detector.

This phenomenon can be modeled using statistics: a sum of phasors is seen as random walk in a 2D grid. This model gives a first approximation of the probability distribution of intensity of the speckles, yielding an exponential decreasing probability. When the size of the pixels used for capturing the speckles cannot be neglected, a more detailed model is required, accounting for the overlap of multiple speckles at each pixel [2]. Figure 2 presents the possible shapes for the probability distribution of intensity of the speckles:

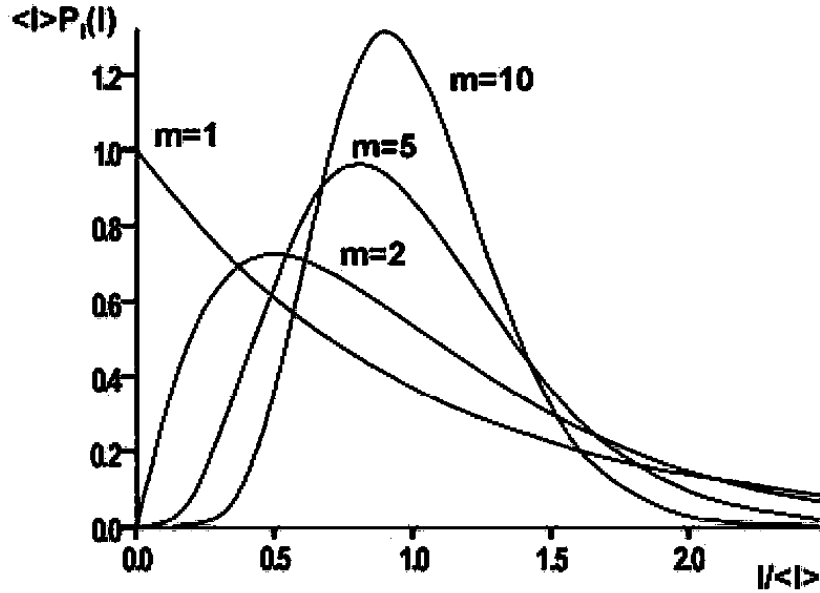


Figure 2: Probability distribution of intensity of the speckles as a function of the parameter m , which is 1 when the speckles are fully resolved and increase with the importance of the relative size of the pixels [2].

With a reference wavefront, interferometry can be performed and employed as a non-invasive testing method. The technique is based on a differential imaging: an object under analysis maybe submitted to a dynamic deformation. Interference speckle images are obtained at different times. Performing the subtraction of the images reveals an interference pattern. This pattern contains the wrapped phase information of the relative deformation between the moments of at which each picture was taken [3].

2 Materials and Methods

A HeNe laser (543 nm) was used as the coherent light source. Since this laser is pumped with high voltage, its wavefronts tend to not be very stable, which is not ideal for a interference experiment. Figure 3 presents the components used for performing spatial filtering of the laser before usage.

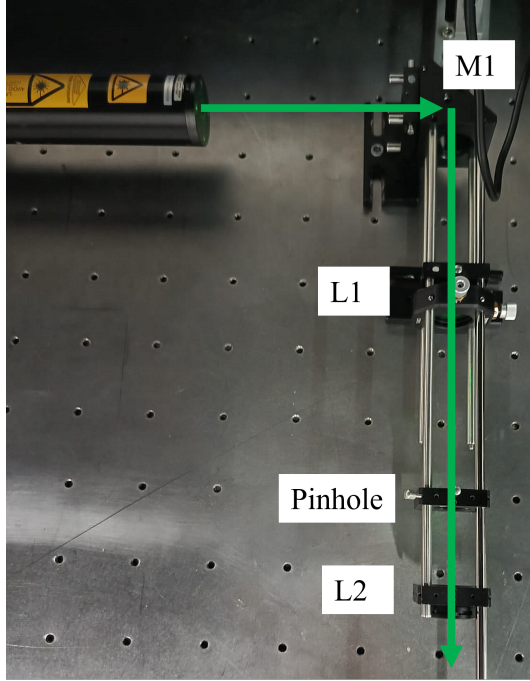


Figure 3: Spatial filtering of the light source. M1 is a mirror used for changing the direction of the laser; L1,2 are lenses used respectively for focusing and collimating the beam, before and after the small pinhole, used for the spatial filtering at the Fourier plane.

The setup used for performing the ESPI is depicted in Figure 4. Except for mirrors used for beam guiding, the main elements of the setup are: BS1, used for separating the incoming beam into two, the reference and the one reflected by the target object. The reference passes through an attenuator in order to decrease its intensity and maximize the contrast of the interference pattern. The other beam passes through an aperture, which controls the spatial frequency of the speckle patterns and is collected by a lens of 40 mm of focal length, imaging the object onto a CCD detector. The BS2 finally combines the two beams composing a, so called, subjective speckle pattern formation.

The different target objects used during the experiment are depicted in Figures 5-7. The first target is an aluminum strip covered with matte paper (side not shown in Figure 5), which had a precision gauge pushing at a position 38 mm above the rigid portion of the part. The precision gauge was positioned about 0.005 mm further against the stripe between every picture.

The second target, Figure 6, is also covered with matte paper, but with an extra feature: millimetric marks. The target is mounted on a device that allows XY movements along a vertical plane. The graduation is important for comparing the results of the in-plane movement calculated from the correlation of the speckle patterns with the actual displacement.

Finally, the third target, Figure 7, is the sticky side of a blue electric tape. It was chosen for being easily deformable and highly elastic when compared to other available materials from the laboratory. For this part of the experiment, the gauge was used to poke the tape and then retracted. In a rate of approximately 2.5 pictures per second were successive taken while the poked portion of the tape relaxed back to its original position.

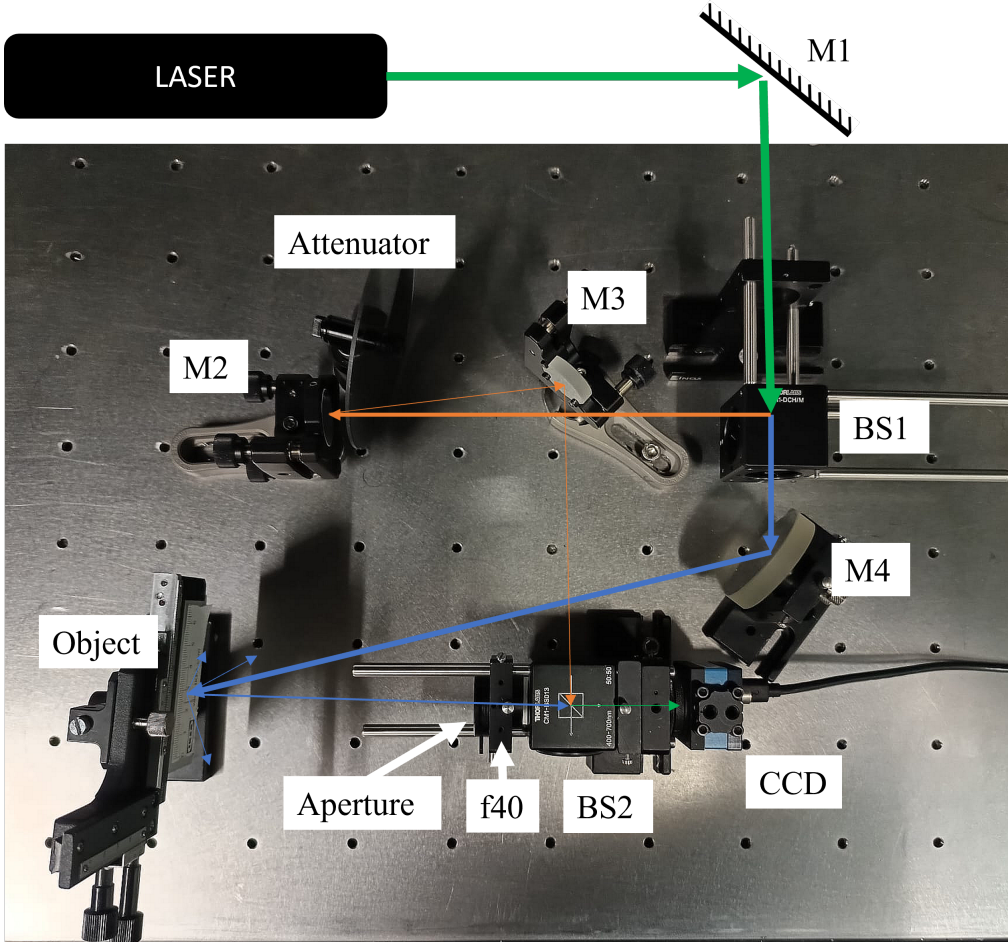


Figure 4: Experimental setup for performing the ESPI. M1-4 are mirrors; BS1,2 are 50% beam splitters; and f40 is a lens used for imaging the object onto the CCD detector.

A summary of the steps required for recovering the relative 3D deformation of the surface from the acquired pictures is depicted in Figure 8:

1. Two pictures are selected and have their pixel value transformed to double. The interference pattern is recovered by evaluating the absolute value of their pixel-to-pixel difference.
2. In a context with several pictures taken, a mean value is calculated over all samples and used to estimate the systematic errors in the background. The calculated interference pattern is then cleaned by dividing pixel-to-pixel by the mean background.
3. Using a local average followed by a binary threshold algorithm, the valleys of the interference pattern are identified.
4. By inspection, a reference pixel is chosen as the top of the deformation and from their, the following valleys are characterized in order. A similar procedure is performed for peaks of the interference pattern.
5. The results from the peaks and valleys are combined.
6. After some extra manual corrections, a polynomial fit (order 10 in x, y and xy) is used for smoothening the data. Finally, the 3D shape of the relative deformation is plotted using the cleaned interference pattern as texture.

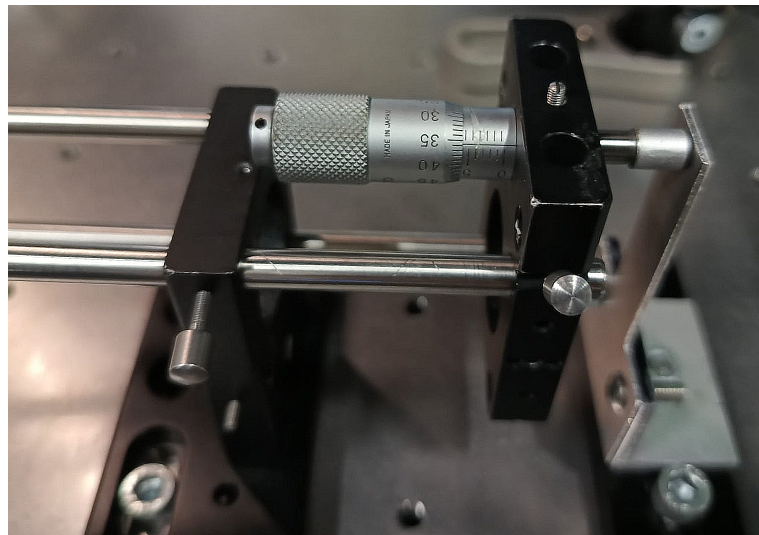


Figure 5: Device used for bending the target object.

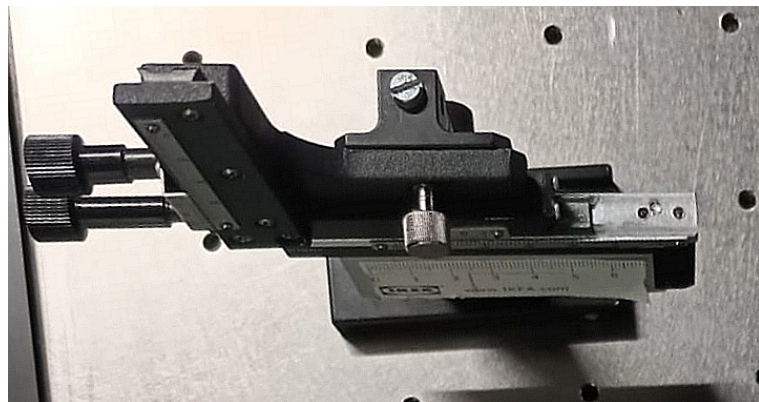


Figure 6: Device used for moving the target object horizontally.

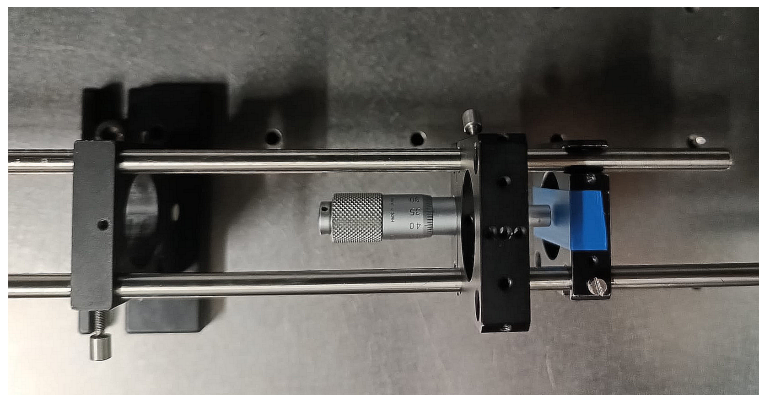


Figure 7: Device used for poking the target object.

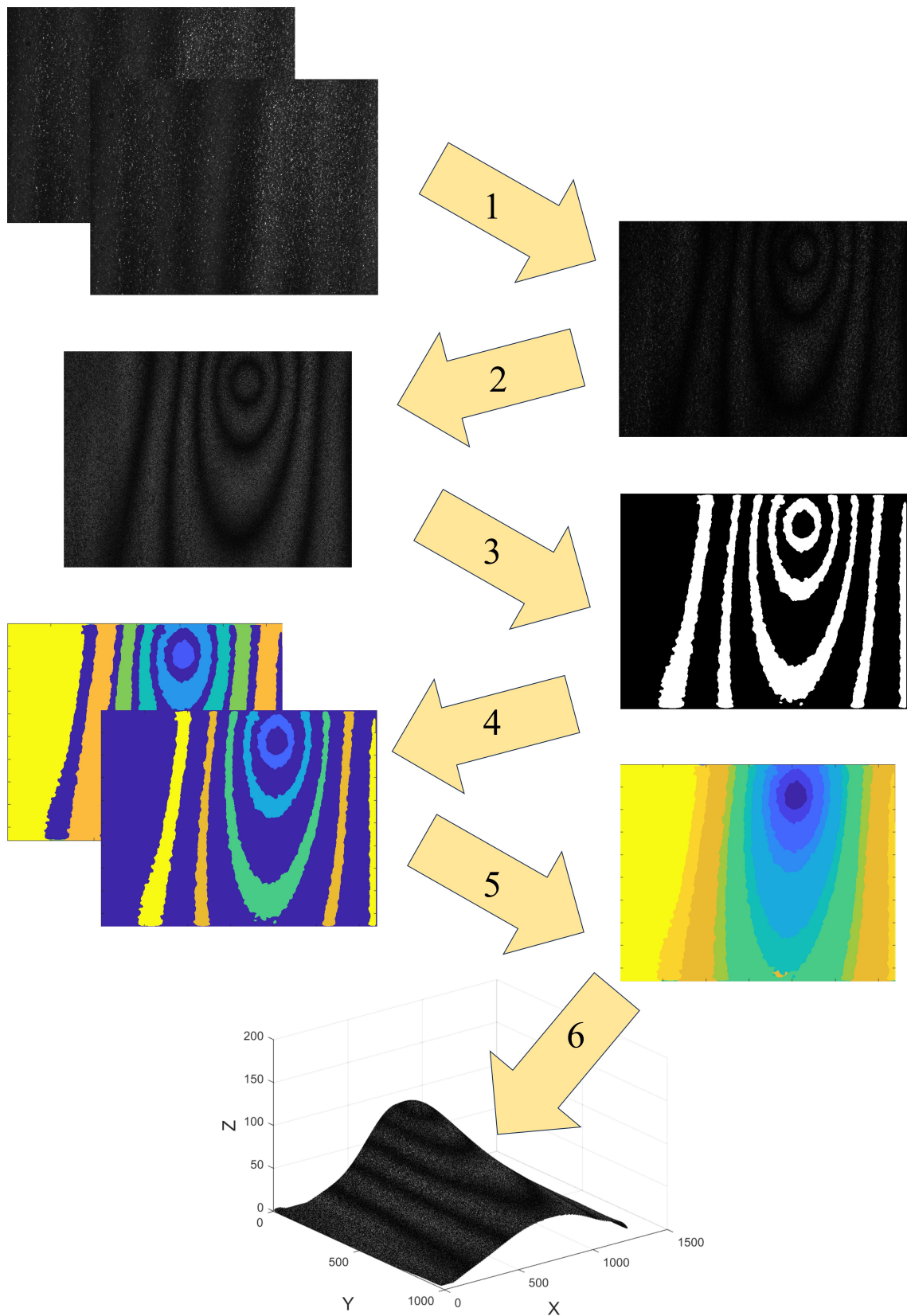


Figure 8: Method used for transforming the captured pictured into 3D images of the surface deformation.

3 Results and Discussion

An undesired interference pattern was observed in the images collected by the CCD. Fortunately, due to the differential character of this experiment, this systematic error was easily mitigated and it did not interfere on the results. After some investigation, its cause was narrowed down to the BS1: a double reflection was creating vertical lines in the reference beam profile.

Figure 9 is a diagram showing how the extra angle α caused by the advance of the precision gauge could be evaluated: the interference pattern extends for $L = 6.7$ mm; the distance $b - a = d$ can be estimated by the number of fringes of the interference (each transition from high intensity to low intensity is equivalent to $\lambda/4$). Since α is fairly small, it can be approximated in radians as d/L .

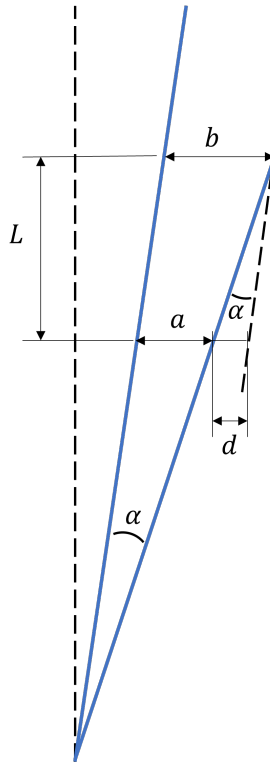


Figure 9: Method used for calculating the extra angle α added by each advance of the precision gauge.

The advance of the precision gauge D , could also be estimated using the same approximation: $D = H\alpha$, where H is 38 mm (distance of the tip of the precision gauge to the axis of rotation of the strip). Table 1 presents the average values of α and D over the interference patters found in Figure 14 in the Appendix. As expected, the values are fairly close to 0.005 mm, or half of the graduation of the instrument.

Table 1: Estimated displacement of the precision gauge for different set of pictures.

	13-16	14-17	15-18	16-19
average α in μrad	121 ± 8	111 ± 8	116 ± 8	139 ± 8
average D in μm	4.6 ± 0.3	4.2 ± 0.3	4.4 ± 0.3	5.3 ± 0.3

Figure 15 (a) and (b) in the Appendix, present an example of the crops of the pictures used for 2D cross-correlation. For each speckle pattern measurement a corresponding image was taken without the laser light as a reference for comparison (Figure 16 (a) and (b) also in the Appendix). After performing each cross-correlation, a local maximum was observed and, after normalization, it became a global maximum of cross-correlation, as shown in Figure 10 (a) and (b) respectively.

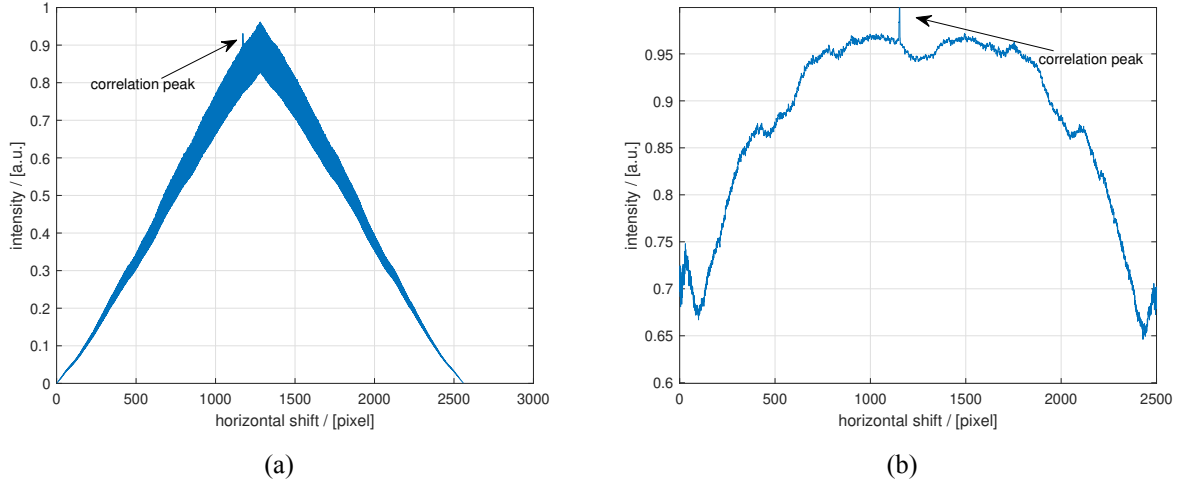


Figure 10: Plot of the 2D correlation along the full vertical overlap: (a) not normalized and (b) normalized using the area of overlap.

The summary of the estimation of the horizontal displacement using each of the methods is presented in Figure 11. A good agreement is observed between each of the techniques. The consistent overestimation of the displacement using maximum correlation suggests a possible systematic error, but its cause remains unclear.

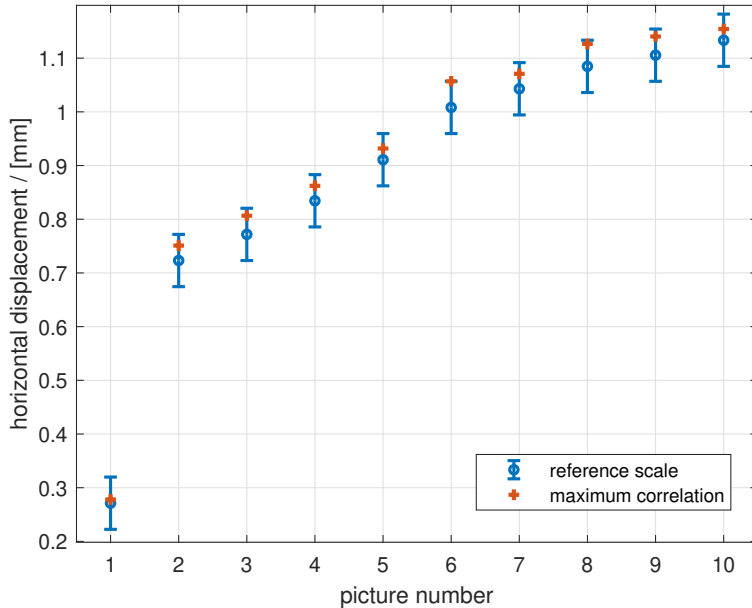


Figure 11: Comparison of the horizontal movement of the target calculated using the reference scale vs. calculated using speckle pattern correlation.

Using ESPI it was possible to calculate the deformation field over the surface of the third target with uncertainty of $\lambda/8$, equivalent to half of the stripe of the interference pattern or about 70 nm. Figure 12 presents data about the evolution of the relative position of the peak of deformation created by the poking device:

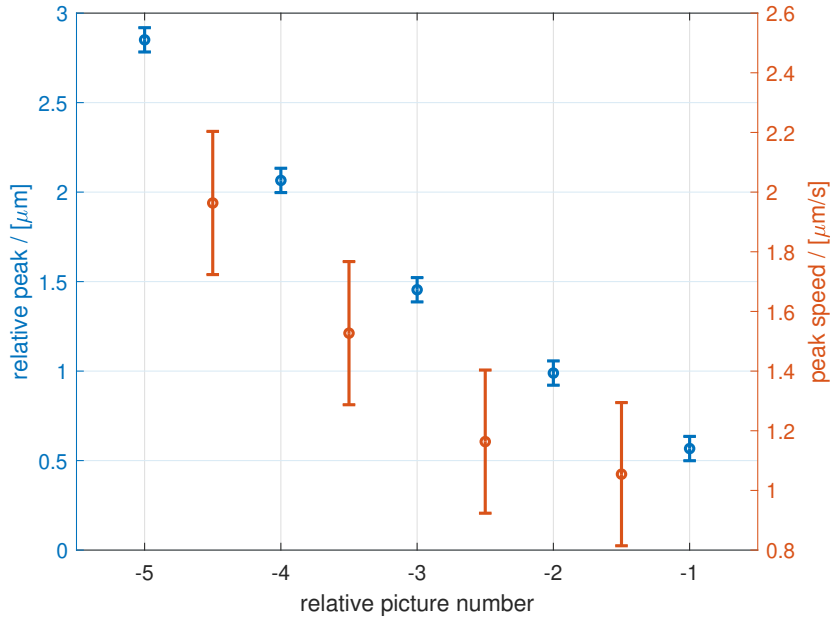


Figure 12: Relative advance of the deformation peak position as a function of the relative picture, where picture 124 was taken as reference (in blue); and instantaneous speed calculated using each consecutive pair of data-points (in orange).

The plot reveals not only a steady decrease of the relative peak magnitude, but also a downwards trend of the speed. This is a characteristic behavior of polymers after being unloaded [1] commonly observed in a punch creep recovery test. In the Appendix, Figures 17 and 18 depict, respectively, the interference pattern caused by this 3D deformation and the actual 3D deformation plot using the interference pattern as texture. In order to visualize the animation Adobe Acrobat Reader is recommended.

At last, a visualization of the pixel intensity distribution due to speckle pattern is presented in Figure 13. A qualitative comparison to Figure 2 indicates that the size of the pixels were non negligible, so that the experiment were be benefited by reducing the aperture diameter.

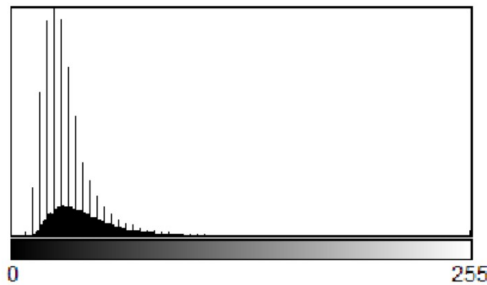


Figure 13: Histogram of the pixels intensity in a speckle pattern picture.

4 Conclusion

This laboratory practice was a successful demonstration of the high resolution tool for deformation mapping that ESPI is. Using a simple algorithm for unwrapping the phase, a deformation map of a 59 mm^2 region with uncertainty of only $\lambda/8 \approx 70\text{nm}$ was obtained. As a down side it is worth mentioning that the technique requires precision on the decision of the reference pixel which has to be done manually; in other hand, using artificial intelligence for image processing and/or more complex algorithms, much higher accuracy can be obtained without need for setup change.

The cross-correlation technique was also explored, producing higher accuracy than a manual pixel counting ($7 \mu\text{m}$ vs $50 \mu\text{m}$). Without a magnification module or a increase in pixel density at the CCD detector, this technique cannot deliver better results, since its already pixel limited.

References

- [1] J. Calaf-Chica, P. M. Bravo Díez, and M. Preciado Calzada. Viscoelasticity and the small punch creep recovery test: Numerical analysis and experimental tests on the applicability for polyvinyl chloride (pvc). *Mechanics of Materials*, 161:104016, 2021.
- [2] J. W. Goodman. *Statistical Properties of Laser Speckle Patterns*, volume 9. Springer Science, 1975.
- [3] Z. Nazarchuk, L. Muravsky, and D. Kuryliak. Digital speckle pattern interferometry for studying surface deformation and fracture of materials. In *Optical Metrology and Optoacoustics in Nondestructive Evaluation of Materials*, volume 242 of *Springer Series in Optical Sciences*, pages 149–217. Springer Singapore Pte. Limited, Singapore, 2023.
- [4] C. A. Sciammarella and F. M. Sciammarella. Speckle patterns and their properties. In *Experimental Mechanics of Solids*, pages 547–582. Wiley, United Kingdom, 2012.

A Appendix

A.1 2D interference patterns

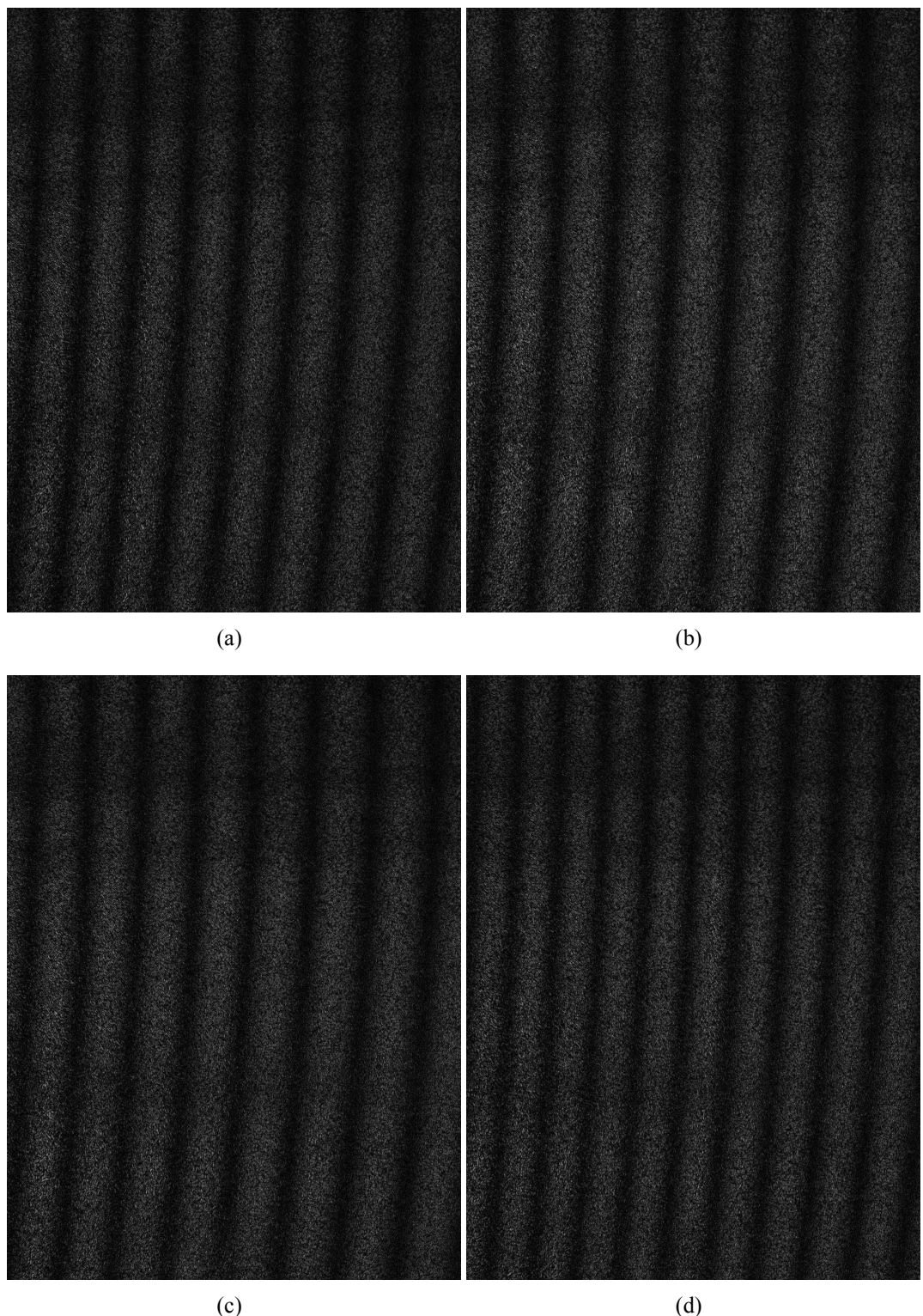
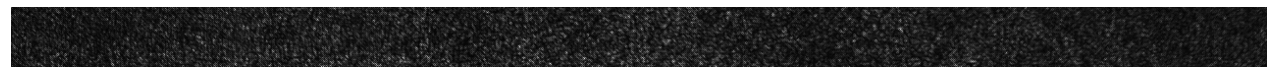
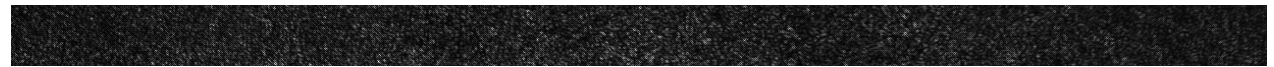


Figure 14: Interference pattern corresponding to the 2D deformation of the aluminum strip. Each figure from (a) to (d) was generated by the processing of picture n and n+3, $n \in \{13, 14, 15, 16\}$.

A.2 2D cross-correlation



(a)

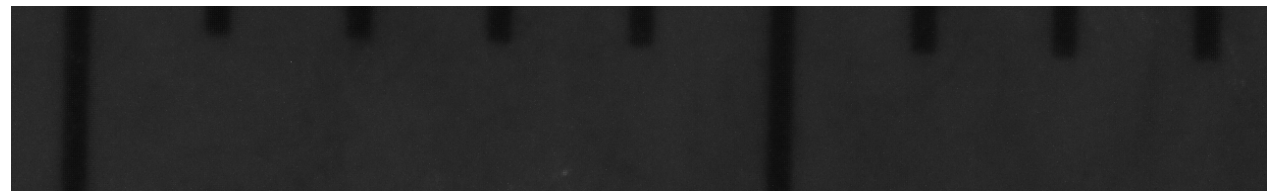


(b)

Figure 15: Crop of the pictures (a) 67 (reference picture) and (b) 65 used for speckle pattern 2D correlation. The crop correspond to pixels (61:121,:) using Matlab syntax and were chosen for not presenting noticeable reference features.



(a)



(b)

Figure 16: Crop of the pictures (a) 66 (reference picture) and (b) 64 used for manual estimation of the horizontal displacement. The crop correspond to pixels (773:960,:) using Matlab syntax. The distance was estimated by the advance of the first half centimeter mark.

A.3 3D interference patterns and deformations

Figure 17: Interference pattern corresponding to the 3D deformation of the electric tape displayed in correct frame rate. Each figure was generated by the processing of picture n and 124, $n \in 114, 123$.

Figure 18: 3D deformation corresponding of the electric tape displayed in correct frame rate. Each figure was generated by the processing of picture n and 124, $n \in 119, 123$.